Development and characterisation of a $Y_2Ti_2O_7$-based glass-ceramic as a potential oxidation protective coating for titanium suboxide (TiO_x)

Fabiana D'Isanto[1], Federico Smeacetto[1], Hans-Peter Martin[2], Richard Sedlák[3], Maksym Lisnichuk[3,4], Andreas Chrysanthou[5], Milena Salvo[1]*

[1] Department of Applied Science and Technology, Politecnico di Torino, Corso Duca degli Abruzzi 24, 10129, Turin, Italy.
[2] Fraunhofer Institute for Ceramic Technologies and Systems IKTS, Winterbergstraße 28, 01277 Dresden, Germany.
[3] Institute of Materials Research, Slovak Academy of Sciences, Watsonova 47, Košice, 04001, Slovakia.
[4] Institute of Physics, Faculty of Science, P. J. Šafárik University, Park Angelinum 9, Košice, 04001, Slovakia.
[5] School of Physics, Engineering and Computer Science, University of Hertfordshire, College Lane, Hatfield, Herts AL10 9AB, UK.

*Corresponding author: Milena Salvo, milena.salvo@polito.it

Abstract

A silica-based glass-ceramic, with $Y_2Ti_2O_7$ as the major crystalline phase, is designed, characterised and tested as an oxidation-protective coating for a titanium suboxide (TiO_x) thermoelectric material at temperatures of up to 600 °C. The optimised sinter-crystallization treatment temperatures are found to be 1300 °C and 855 °C for a duration of 30 min, and this treatment leads to a glass-ceramic with cubic $Y_2Ti_2O_7$ and $CaAl_2Si_2O_8$ as crystalline phases. An increase of ~270 °C in the dilatometric softening temperature is observed after devitrification of the parent glass, thus further extending its working temperature range.

Excellent adhesion of the glass-ceramic coating to the thermoelectric material is maintained after exposure to a temperature of 600°C for 120 h under oxidising conditions, thus confirming the effectiveness of the T1 glass-ceramic in protecting the TiO_x material.

Keywords: glass-ceramics; oxidation protective coating; titanium suboxides

1. Introduction

Despite their low carrier mobility, in comparison to other thermoelectrics, oxides are an interesting class of thermoelectric materials (TE). Their moderate stability at high temperatures is particularly advantageous when temperatures in excess of 400 °C can be used for thermoelectric energy conversion. In addition, certain oxides, such as ZnO and TiO_x, are abundant in the earth's crust, and are non-hazardous (NbO_x, TiO_x) and cost-effective (TiO_x) [1,2]. $NaCo_2O_4$, $Ca_3Co_4O_9$ and $Bi_2Sr_2Co_2O_9$ layered cobaltites have high Seebeck coefficients and low thermal conductivities [3–5], and have frequently been discussed for use as p-type thermoelectric materials, while $SrTiO_3$, $CaMnO_3$ and titania-based materials are candidates for n-type thermoelectrics [4,6,7]. The Magnéli phases, with the Ti_nO_{2n-1} and n >4 formula [8], have an electrical conductivity range of 10^1 to 10^3 Ωcm, a Seebeck coefficient range of between 20 and 200 $\mu V \cdot K^{-1}$ and a thermal conductivity range of between 2 and 3 $W \cdot (m \cdot K)^{-1}$, thus making them attractive for moderate thermoelectric conversion [2,9]. Additionally, titanium suboxides are the most economical of all oxides, due to their low raw material and manufacturing costs. Even though TiO_x only achieves a figure of merit (ZT) of between 0.13 and 0.33 at temperatures of around 1000 K [10], it has attracted a great deal of attention as a TE material [7],[11–14]. The reasons for this lie in its unlimited availability, low cost and its cost-effective manufacturing technology.

One practical drawback to the use of TiO_x as a TE ceramic material for high temperature devices is its strong oxidation, which can result in the formation of the stable TiO_2 oxide. According to Diamanti et al [15], the oxidation of titanium suboxides begins at temperatures above 400°C. Since titanium oxides conduct oxygen, the oxide layers are not able to protect the bulk ceramic, as is the case of silicon dioxide, which can protect SiC and Si_3N_4 up to 1400 °C. Thus, the development of suitable protective coatings for titanium suboxide TE legs is fundamental in order to prevent the degradation of the thermoelectrical properties at a high temperature. In this work, a new silica-based glass-ceramic coating containing $Y_2Ti_2O_7$ has been designed, and its ability to protect TiO_x against oxidation at temperatures of up to 600°C has been investigated.

2. Materials and methods

The glass-ceramic coating, referred to as T1, was developed with the support of the SciGlass® software (Science Serve GmbH, Sciglass 6.6 software, Newton, Massachusetts, USA). The parent glass was

produced, by means of conventional melting and casting, from the following high-purity grade raw materials: SiO_2 (Sigma Aldrich, 99.5 % purity) with 41.48 mol%, Al_2O_3 (Alfa Aesar, 99.9 % purity) with 16.29 mol%, TiO_2 (Sigma Aldrich, ≥ 99% purity) with 20.79 mol%, Y_2O_3 (Sigma Aldrich, 99.99 % purity) with 5.52 mol%, CaO (precursor $CaCO_3$ Sigma Aldrich, 99 % purity) with 7.40 mol %, K_2O (precursor K_2CO_3 Sigma Aldrich, 99.5 % purity) with 1.82 mol% and Na_2O (precursor Na_2CO_3 Sigma Aldrich, 99.5 % purity) with 6.70 mol%. This mixture was melted in a Pt-Rh crucible inside an electric furnace (LHT418PN2, Nabertherm GmbH, Lilienthal/ Bremen, Germany) in air at 1500 °C for 1 h and at 1550 °C for 30 min. The melt was cast onto a metal plate, and the glass was subsequently ball-milled and sieved (particle size < 38 μm). The T1 glass powders were characterised by means of differential thermal analysis (DTA, Netzsch DTA 404 PC) and through the use of heating-stage microscopy (HSM, Hesse Instruments, Harzgerode Germany), using a heating rate of 10 °C/min.

The titanium suboxide TiO_x was produced at the Fraunhofer Institute for Ceramic Technologies and Systems, IKTS, Germany, starting from TiO_2 powder (Kronos 3025, KRONOS Worldwide, Inc., the USA) and TiC (STD-120 A, H.C. Starck GmbH, Germany). The TiO_2 and TiC powders were mixed and ball-milled for 4 hours and subsequently heated at 1200 °C under an argon atmosphere to obtain TiO_x. Ball milling of the TiO_x powder and 50 mol% TiO_2 powder (Crenox 8602) was then carried out with the addition of methyl acrylate and wax binders (5.5 mol%). The powder was subsequently drypressed into compacts using an isostatic pressure of 150 MPa. This was followed by pyrolysis (debindering) of the pressing aids at 1000 °C for 1 h. The samples were heated to 1000 °C at a rate of 3 °C/min under flowing Ar. Finally, the samples were sintered at 1300 °C under flowing N_2, using a heating rate of 5 °C/min and with a dwell time of 2 hrs.

The T1 glass powder (<38 μm size) was dispersed in ethanol (1:2 weight ratio) and the slurry was then deposited manually onto the TiO_x substrate using a spatula. The coating deposition thermal treatment, which was based on the results of DTA and HSM analyses, was carried out at 1300 °C for 10 min (10 °C/min) and this was followed by cooling to 855 °C, a 30 min dwell at 855 °C, and by cooling to room temperature (natural furnace cooling) in a tubular furnace (STF 16/ 180, Carbolite, Hope Valley, the UK) under continuous flowing Ar.

The microstructures of the coated samples were examined using a field emission scanning electron microscope (FE-SEM, Merlin electron microscope, ZEISS, Oberkochen, Germany) equipped with an energy-dispersive spectrometer (EDS) (EDS, Zeiss Supra TM 40, Oberkochen, Germany). Furthermore, some samples were analysed, by means of a transmission electron microscope (TEM) JEOL 2100F UHR, equipped with a Schottky field emission gun. Images were taken in bright field imaging mode, while the selected area electron diffraction technique (SAED) was used for the investigation of the reciprocal space. The elemental composition of the samples was analysed, by means of EDS spectrometry, employing an Oxford Instruments SDD detector Xmax80. The samples were prepared by mechanical pre-thinning and ion milling using a Gatan PIPS model 691.

The X-ray diffraction (XRD) patterns were obtained using an X'Pert Pro MRD diffractometer, with Cu Kα radiation (PANalytical X'Pert Pro, Philips, Almelo, The Netherlands), and with the aid of X-Pert HighScore software, while the phases were identified using the JCPDS database provided by PDF-2 ICDD (International Centre for Diffraction Data, Newton Square, Pennsylvania, the USA). The coefficient of thermal expansion (CTE) and the dilatometric softening point of T1 were measured (before and after the deposition heat-treatment) using a dilatometer (Netzsch, DIL 402 PC). The oxidation resistance of the uncoated and coated TiO_x was assessed by heating samples at 600 °C for 120 h in air in a muffle furnace (Manfredi OVMAT 2009, Pinerolo, Italy); the samples were heated from room temperature to 600 °C at a heating rate of 10 °C/min and were cooled to room temperature (natural furnace cooling) after a 48 h dwell time. An additional 72 h treatment at 600 °C in air was carried out. X-ray diffraction analysis was conducted on both the uncoated and coated samples after oxidation tests (the coating of the coated sample was removed before the analysis).

3. Results and Discussion

The as-cast T1 glass was opaque and white in colour. Figure 1 shows an SEM image of the microstructure of the T1 glass within which two phases can be detected: (i) a continuous dark matrix and (ii) specks of a brighter uniformly-dispersed round-shaped phase of a size ranging from 200 to 250 nm. Three different hypotheses were considered to explain the development of this microstructure:

(i) the initial formation of a primary crystal phase during the cooling of the glass melt followed by the generation of spherical nano-crystals;

(ii) glass-phase separation, which led to the formation of spheroids distributed in a homogeneous glassy matrix;

(iii) glass-phase separation caused the formation of glass droplets in which nanometric sized primary crystals formed.

The opaque appearance of the as-cast T1 is characteristic of phase-separated glasses. However, the XRD pattern of the as-cast T1, shown in Figure 2(a), revealed the presence of some low intensity peaks that were attributed to a crystalline phase, thus supporting hypotheses (i) and/or (iii).

A further examination of the microstructure was carried out, using TEM and SAED analyses on the as-cast glass. Figure 3a shows that two different regions can be detected in the sample: a bright region with darker rounded areas (region A) and a dark region containing large brighter circular areas where much smaller dark rounded particles are visible (region B). Electron diffraction patterns, taken from different areas of region A, showed that the bright phase and some of the darker spherical areas within the bright region are amorphous, while some of them are crystalline. The SAED analysis of the dark area of region B showed that it is a crystalline phase, while the bright circular areas and the very small dark circular phase within these areas showed diffuse rings, which are typical of amorphous phases. All the diffraction patterns of the crystalline areas corresponded to cubic phase $Y_2Ti_2O_7$, thus confirming the XRD analysis. Furthermore, the EDS mapping of selected areas of regions A and B pointed out that the darker areas are Ti- and Y-rich, while the bright areas are Si-rich (Figure 3b). The distinctly separated spherical droplets that characterise this microstructure can be attributed to a glass phase separation, resulting from the nucleation and growth of a Ti- and Y- rich glass phase (darker droplets), in which the primary $Y_2Ti_2O_7$ crystals formed at a nanometric size, and a silica-rich second glass phase.

Thermal analyses (DTA and HSM) were carried out to study the sinter-crystallisation of the coating material. Figure 4 (black curve) shows the DTA curve of the T1 parent glass. It can be observed that T_g is around 750 °C, while three exothermic peaks (each corresponding to the formation of a crystalline phase) and one endothermic peak (corresponding to the melting temperature) can be detected at higher temperatures, as reported in Table 1. As mentioned above, the XRD analysis in Figure 2a for the as-cast T1 glass sample shows the presence of a highly amorphous phase along with a small number of peaks of extremely low intensity. The intensity of the peaks of the as-cast bulk material increases, following the 30-minute heat-treatment at 855 °C, which corresponds to the temperature of the first crystallisation peak,

$T_{p1,}$ and more peaks are evident, as can be seen in Figure 2b. At the same time, it can be noted that a significantly smaller amount of the residual glassy phase is present. The observed peaks in Figure 2b correspond to the defect cubic fluorite $Y_2Ti_2O_7$ phase with an *Fm3m* space group.

Figure 4 (blue curve) shows the sintering behaviour of the T1 glass, as investigated by means of hot-stage microscopy (HSM). The observed characteristic points are: (i) a temperature (T_{FS}) of 835°C, which represents the temperature at which linear shrinkage of the glass starts, (ii) the maximum shrinkage temperature (T_{MS}) at 1080°C, (iii) the softening/deformation point (*DT*), which is the temperature at which the first signs of softening are observed (1126 °C), (iv) the sphere temperature (*ST*), which is the temperature at which the height of the sample is equal to the width of the base (1294 °C), (v) the half-ball point (T_{HB}), which is the temperature at which the height of the sample is half the width of the base (1342 °C) and (vi) *T* flow (T_F), the temperature at which the height of the sample drops to below one-third of the base (1394 °C). Since the crystallisation phenomenon can reduce the densification rate of the coating material, by means of a viscous flow, the correct order of events is likely to consist of the maximum shrinkage first being reached and crystal growth subsequently being induced in order to produce the glass-ceramic. However, as observed in Figure 4, the onset of the first crystallisation peak in the DTA plot almost overlaps the first shrinkage temperature measured by means of hot-stage microscopy; therefore, the two phenomena are not as independent, as would instead be desirable. Considering these results, the coating deposition heat-treatment that was chosen was 1300 °C for 10 min, followed by a heat-treatment at 855 °C for 30 min (10 °C/min heating rate) under flowing Ar.

The sintering of a T1 glass pellet at 1300°C for 10 min, followed by a heat-treatment at 855°C for 30 min, yielded additional peaks in the XRD scan, as shown in Figure 2c. The XRD peaks in Figure 2c correspond to the cubic pyrochlore $Y_2Ti_2O_7$ phase that exhibits the *Fd3m* space group, which was the main phase that was present, and to an additional $CaAl_2Si_2O_8$ anorthite phase. The pyrochlore and fluorite crystal structures follow a face-centred cubic modification, but with different space groups, as indicated above. The main difference in their XRD patterns is that the (111), (331) and (511) reflections are absent from the fluorite pattern. The ideal pyrochlore $Y_2Ti_2O_7$ structure can be described to be in the form of $A_2B_2O_7$, in which the atoms of each metal are strictly situated at specific crystallographic positions [16]. The yttrium atoms occupy the A-sites and the titanium atoms the B-sites. A change in the defect fluorite crystal structure may take place when the yttrium and titanium atoms are randomly

distributed within the crystal lattice. An estimate of the degree of cationic distortion at the B site of the pyrochlore phase can be obtained by calculating the ratio of the intensity of the (400) peak to that of the (331) peak [17]. The (400):(311) intensity ratio decreases as the Ti/Y ratio increases; the presence of more titanium in the structure in fact tends to reduce cationic distortion. Furthermore, it should be noted that the indexing of the peak at 2θ~32° is still uncertain; this peak may be attributed to hexagonal Y_2TiO_5 although previous studies [18, 19] have reported that the transformation of α-orthorhombic yttrium titanium oxide to the ß- hexagonal phase occurs at about 1330 °C, which is a higher temperature than the ones used in the present study. In addition, it was not possible to identify the phase corresponding to the peak at 2θ~52.5°.

The microstructure of a sintered T1 glass-ceramic pellet and the related EDS elemental maps are shown in Figure 5. The main crystalline phase, $Y_2Ti_2O_7$ pyrochlore has a morphology similar to the microstructure that was reported by Wei *et al.* [20] and by Kong *et al.*[21]. $Y_2Ti_2O_7$ has a coefficient of thermal expansion of ~$8.4 \cdot 10^{-6}$ K^{-1} in the 300-1000 °C range [22], a value that is similar to that of titanium suboxide (7-$9 \cdot 10^{-6}$ K^{-1}) [23]. Furthermore, the $Y_2Ti_2O_7$ pyrochlore is chemically stable at high temperatures, has a low thermal conductivity [22] and, consequently, is a promising candidate material for the oxidation protection of TiO_x.

Together with the residual glassy phase (dark phase in Figure 5a) and $Y_2Ti_2O_7$ crystals, needle-like crystals are also present. The EDS maps show that the elongated needle-like phase contains Ca, Al, Si and O, and can be attributed to the $CaAl_2Si_2O_8$ anorthite phase that was also detected in the XRD analysis (Figure 2c).

A further examination of the glass-ceramic microstructure was carried out using TEM and SAED analyses (Figure 6). The diffraction patterns of the black crystals confirmed that they are the cubic $Y_2Ti_2O_7$ phase, while the light-grey crystals are the triclinic $CaAl_2Si_2O_8$ phase. Furthermore, it can be seen, at higher magnifications (Figure 6b), that there are very small particles in some regions of the light amorphous area; the SAED analysis confirmed that these particles are hexagonal phase Y_2TiO_5 in an amorphous matrix.

The coefficient of thermal expansion of the T1 parent glass, as measured using dilatometry, is 8.6×10^{-6} K^{-1} between 200 °C and 500 °C, while the dilatometric softening point is 792 °C (Figure 7, curve 1). It can be observed, from the dilatometry curve of the sintered T1 glass-ceramic (Figure 7, curve 2), that the CTE of T1 increased slightly following the heat treatment, that is, from $8.6 \cdot 10^{-6}$ K^{-1} to $9.1 \cdot 10^{-6}$ K^{-1}, and that the

dilatometric softening temperature, T_d, increased significantly from 792 °C, for the parent glass, to 1081 °C for the glass-ceramic. Therefore, the heat-treatment that was selected for the coating deposition clearly led to a glass-ceramic with improved refractory properties and with an extended working temperature range.

TiO_x samples were then coated with T1, using the procedure described in the experimental section and the same heat-treatment discussed above. Figure 8 shows a cross-section of a T1 glass-ceramic coated TiO_x; it is evident that the coating adheres to the substrate very well and that there are no visible cracks or delamination phenomena at the coating/TE interface, where a 1-1.5 μm thick reaction layer is visible. The distribution of the crystalline phases within the glassy matrix is not homogeneous. It can be observed that small bright grains of $Y_2Ti_2O_7$, with a size of around 1 μm, are homogeneously distributed within the darker glassy phase, close to the interface, while the elongated grains, previously attributed to the $CaAl_2Si_2O_8$ phase, are only visible at a distance of ~20 μm from the coating/TiO_x interface.

The EDS elemental maps of a T1-coated TiO_x cross-section are reported in Figure 9. The large amounts of Si, Na, Al and K detected within the pores of the substrate indicate that the glass phase infiltrated the porous areas at the TiO_x surface and the residual glassy phase does not contain Ti, Y or Ca, at least in sufficient amounts to be detected with this technique. Moreover, the larger concentrations of Y and Ti within the continuous reaction layer at the T1/TiO_x interface suggest that the reaction between TiO_x and T1 led to the formation of $Y_2Ti_2O_7$, the main crystalline phase of the T1 glass-ceramic. The Ca depletion in the coating region close to the interface with the TE is worth noting; the Ca diffused at a distance from this region and this led to the formation of needles of the anorthite phase at a distance of ~20 μm from the interface and even further away. In addition, the EDS line-scan (Figure 10) shows that the Ti content immediately adjacent to the TiO_x is high and decreases at a distance from it, while the level of Y is low at the interface and increases at a distance (zone 1 in Figure 10). It should also be noted that no increase in the amount of oxygen at the interface was observed within TiO_x, so there was no evidence of any TiO_2 formation. The trend of the composition of Ti in the pyrochlore phase, when moving away from the interface with TiO_x, follows an opposite pattern to that of Y for about 0.5 μm and, at that point, the amounts of the two elements seem to become more or less steady. There are two possible reasons for this phenomenon; it may have occurred due to (i) reaction or diffusion of Ti from the TiO_x substrate into the $Y_2Ti_2O_7$ crystalline phase and/or (ii) preferential nucleation of Ti-rich $Y_2Ti_2O_7$ at the interface with TiO_x. The driving force for the

latter is likely to be dictated by the higher chemical compatibility between Ti-rich $Y_2Ti_2O_7$ and TiO_x. However, it is difficult to distinguish which of these mechanisms is likely to dominate and, in fact, both may have taken place at the same time. The composition results of the line scan show reasonably high levels of Ti within $Y_2Ti_2O_7$. This observation confirms that the layer adjacent to TiO_x is a crystalline pyrochlore $Y_2Ti_2O_7$ modification and not a fluorite structure defect, as the latter tends to be characterised by a low Ti/Y ratio. The amounts of Y and Ti within the darker glassy phase (zone 2 in Figure 10) drop significantly adjacent to the reaction layer, while the levels of the residual glassy phase components (Si, Na, K and Al) increase. The line scan analysis also shows high levels of Ti and Y within a small round-shaped crystalline grain (zone 3 in Figure 10), which has been attributed to the $Y_2Ti_2O_7$ phase. It is interesting to note that the Ti and Y levels in the round-shaped particle follow the same trend. This is contrary to the observed behaviour at the interface with TiO_x, where the gradient in the composition of the Ti is opposite that of Y. This further supports the suggestion that the resulting composition of the pyrochlore phase at the interface with TiO_x is dictated either by the chemical compatibility of the two phases or by a reaction between them. As already mentioned above, the amount of Ca is particularly low in the region close to the glass-ceramic/TiO_x interface and, in fact, there is no evidence of any anorthite at the interface. The reason for this is that there is preferential nucleation of the pyrochlore $Y_2Ti_2O_7$ phase, and this is dictated by the reasons stated above.

On the basis of the above results, the T1 glass-ceramic coated TiO_x and the uncoated samples were submitted to a preliminary oxidation test at 600 °C for 120 h in air. Figure 11 shows the cross-section of a coated sample after the oxidation test. The formation of cracks due to thermal stresses was not observed and the microstructure of the glass-ceramic was not affected by the heat treatment; the T1 glass-ceramic has a glass transition temperature > 750°C (as shown in Figure 7) and below the Tg, the glass viscosity is so high that structural rearrangements required for crystal nucleation and growth are unlikely to occur [24]. Furthermore, the reaction layer at the T1/TiO_x interface appear unaffected (Figure 11b) and it can be seen that the excellent adhesion of the coating to the thermoelectric material is maintained, even after a long exposure to severe conditions.

The XRD pattern of the uncoated substrate following the oxidation test (Figure 12a) shows that it completely oxidised to TiO_2. On the contrary, it is encouraging to observe that the XRD pattern of the coated sample after the oxidation test (after removing the outer layers to reveal pristine TiO_x), shown in

Figure 12b, is identical to that of the as-sintered sample (Figure 12 c), thus confirming the effectiveness of the T1 glass-ceramic in protecting the TiO_x material.

Conclusions

A new silica-based glass-ceramic has been designed to protect a TiO_x substrate against oxidation at temperatures of up to 600°C for 120 h. SEM and TEM analyses have shown that the glass-ceramic has a fine microstructure, where the main crystalline phases are $Y_2Ti_2O_7$ and $CaAl_2Si_2O_8$. Moreover, it exhibited excellent thermo-mechanical and chemical compatibility with the substrate, and the heat-treatment that was selected for the coating deposition led to a glass-ceramic with improved refractory properties, thus extending its working temperature range (an increase of ~270 °C of the dilatometric softening temperature was observed after devitrification of the parent glass devitrification).

References

[1] D.K. Aswal, R. Basu, A. Singh, Key issues in development of thermoelectric power generators: High figure-of-merit materials and their highly conducting interfaces with metallic interconnects, Energy Convers. Manag. 114 (2016) 50–67. https://doi.org/10.1016/j.enconman.2016.01.065.

[2] M. Backhaus-Ricoult, J. Rustad, L. Moore, C. Smith, J. Brown, Semiconducting large bandgap oxides as potential thermoelectric materials for high-temperature power generation?, Appl. Phys. A. 116 (2014) 433–470. https://doi.org/10.1007/s00339-014-8515-z.

[3] I. Terasaki, Y. Sasago, K. Uchinokura, Large thermoelectric power in NaCo2O4 single crystals, Phys. Rev. B - Condens. Matter Mater. Phys. 56 (1997) R12685–R12687. https://doi.org/10.1103/PhysRevB.56.R12685.

[4] H. Ohta, K. Sugiura, K. Koumoto, Recent Progress in Oxide Thermoelectric Materials: p-Type Ca3Co4O9 and n-Type SrTiO3−, Inorg. Chem. 47 (2008) 8429–8436. https://doi.org/10.1021/ic800644x.

[5] R. Funahashi, I. Matsubara, S. Sodeoka, Thermoelectric properties of Bi2Sr2Co2Ox polycrystalline materials, Appl. Phys. Lett. 76 (2000) 2385–2387.

[6] H. Wang, W. Su, J. Liu, C. Wang, Recent development of n-type perovskite thermoelectrics, J.

Mater. 2 (2016) 225–236. https://doi.org/10.1016/j.jmat.2016.06.005.

[7] M. Backhaus-Ricoult, J.R. Rustad, D. Vargheese, I. Dutta, K. Work, Levers for thermoelectric properties in titania-based ceramics, J. Electron. Mater. 41 (2012) 1636–1647. https://doi.org/10.1007/s11664-012-2019-4.

[8] S. Andersson, B. Collén, U. Kuylenstierna, A. Magnéli, Phase Analysis Studies on the Titanium-Oxigen System, Acta Chem. Scand. 11 (1957) 1641–1652.

[9] S. Harada, K. Tanaka, H. Inui, Thermoelectric properties and crystallographic shear structures in titanium oxides of the Magnèli phases, J. Appl. Phys. 108 (2010) 083703. https://doi.org/10.1063/1.3498801.

[10] H. Liu, H. Ma, T. Su, Y. Zhang, B. Sun, B. Liu, L. Kong, B. Liu, X. Jia, High-thermoelectric performance of TiO2-x fabricated under high pressure at high temperatures, J Mater. 3 (2017) 286–292. https://doi.org/10.1016/j.jmat.2017.06.002.

[11] S. Conze, A. Poenicke, H.-P. Martin, A. Rost, I. Kinski, J. Schilm, A. Michaelis, Manufacturing Processes for TiO x -Based Thermoelectric Modules: from Suboxide Synthesis to Module Testing, J. Electron. Mater. 43 (2014) 3765–3771. https://doi.org/10.1007/s11664-014-3128-z.

[12] B. Feng, H.-P. Martin, F.-D. Börner, W. Lippmann, M. Schreier, K. Vogel, A. Lenk, I. Veremchuk, M. Dannowski, C. Richter, P. Pfeiffer, G. Zikoridse, H. Lichte, J. Grin, A. Hurtado, A. Michaelis, Manufacture and Testing of Thermoelectric Modules Consisting of B x C and TiO x Elements, Adv. Eng. Mater. 16 (2014) 1252–1263. https://doi.org/10.1002/adem.201400183.

[13] J. Schilm, A. Pönicke, M. Kluge, I. Sichert, H.-P. Martin, A. Michaelis, TiOx Based Thermoelectric Modules – Manufacturing, Properties and Operational Behavior, Mater. Today Proc. 2 (2015) 770–779. https://doi.org/10.1016/j.matpr.2015.05.097.

[14] H.-P. Martin, A. Pönicke, M. Kluge, I. Sichert, A. Rost, S. Conze, K. Wätzig, J. Schilm, A. Michaelis, TiOx -Based Thermoelectric Modules: Manufacturing, Properties, and Operational Behavior, J. Electron. Mater. 45 (2016) 1570–1575. https://doi.org/10.1007/s11664-015-4115-8.

[15] M. V. Diamanti, S. Codeluppi, A. Cordioli, M.P. Pedeferri, Effect of thermal oxidation on titanium oxides' characteristics, J. Exp. Nanosci. 4 (2009) 365–372. https://doi.org/10.1080/17458080902769937.

[16] O. Merka, D. Bahnemann, M. Wark, Improved Photocatalytic Hydrogen Production by Structure

Optimized Nonstoichiometric Y2Ti2O7, ChemCatChem. 4 (2012). https://doi.org/10.1002/cctc.201200148.

[17] Y.H. Li, Y.Q. Wang, M. Zhou, C.P. Xu, J.A. Valdez, K.E. Sickafus, Light ion irradiation effects on stuffed Lu2(Ti2−xLux)O7−x/2 (x=0, 0.4 and 0.67) structures, Nucl. Instruments Methods Phys. Res. Sect. B Beam Interact. with Mater. Atoms. 269 (2011) 2001–2005. https://doi.org/https://doi.org/10.1016/j.nimb.2011.05.036.

[18] N. Mizutani, Y. Tajima, M. Kato, Phase Relations in the System Y2O3-TiO2, J. Am. Ceram. Soc. 59 (1976) 168. https://doi.org/10.1111/j.1151-2916.1976.tb09459.x.

[19] W. Gong, D. Li, Z. Chen, F. Zheng, Y. Liu, Y. Du, B. Huang, Phase equilibria of the TiO2 - Y2 O3 system, Calphad Comput. Coupling Phase Diagrams Thermochem. 33 (2009) 624–627. https://doi.org/10.1016/j.calphad.2009.06.005.

[20] T. Wei, Y. Zhang, L. Kong, Y.J. Kim, A. Xu, I. Karatchevtseva, N. Scales, D.J. Gregg, Hot isostatically pressed Y2Ti2O7 and Gd2Ti2O7 pyrochlore glass-ceramics as potential waste forms for actinide immobilization, J. Eur. Ceram. Soc. 39 (2019) 1546–1554. https://doi.org/10.1016/j.jeurceramsoc.2018.11.012.

[21] L. Kong, Y. Zhang, I. Karatchevtseva, Preparation of Y2Ti2O7 pyrochlore glass-ceramics as potential waste forms for actinides: The effects of processing conditions, J. Nucl. Mater. 494 (2017) 29–36. https://doi.org/10.1016/j.jnucmat.2017.07.004.

[22] S.T. Nguyen, T. Nakayama, H. Suematsu, T. Suzuki, M. Takeda, K. Niihara, Low thermal conductivity Y2Ti2O7 as a candidate material for thermal/environmental barrier coatings, Ceram. Int. 42 (2016) 11314–11323. https://doi.org/https://doi.org/10.1016/j.ceramint.2016.04.052.

[23] J.K. Gill, O.P. Pandey, K. Singh, Role of sintering temperature on thermal, electrical and structural properties of Y2Ti2O7 pyrochlores, Int. J. Hydrogen Energy. 36 (2011) 14943–14947. https://doi.org/10.1016/j.ijhydene.2011.02.138.

[24] V.M. Fokin, E.D. Zanotto, N.S. Yuritsyn, J.W.P. Schmelzer, Homogeneous crystal nucleation in silicate glasses: A 40 years perspective, J. Non. Cryst. Solids. 352 (2006) 2681–2714. https://doi.org/10.1016/j.jnoncrysol.2006.02.074.

Figures

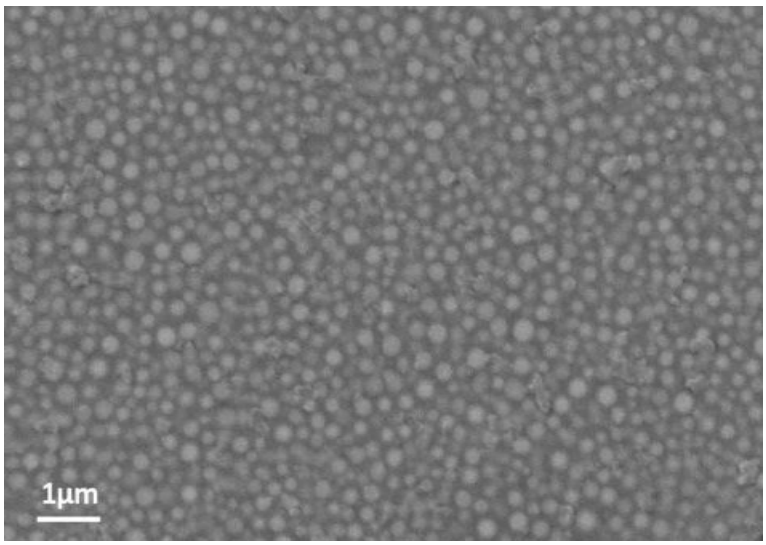

Figure 1: SEM image (BSE) of the as-cast T1 bulk.

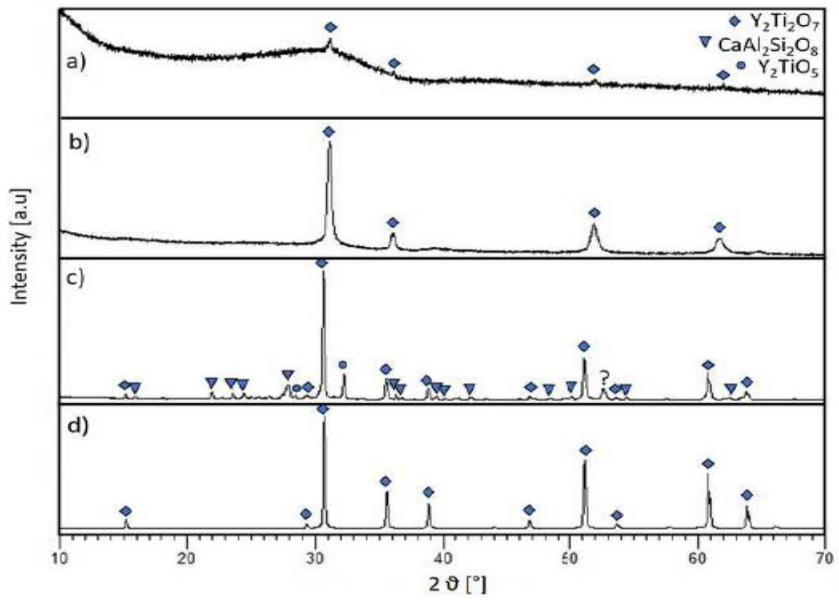

Figure 2: X-ray powder diffraction pattern of (a) as-cast T1, (b) T1 bulk heat treated at 855 °C for 30 min, (c) a T1 pellet sintered at 1300 °C for 10 min followed by a heat-treatment at 855 °C for 30 min. The simulated XRD pattern of $Y_2Ti_2O_7$ from PDF card no. 00-042-0413 is reported in (d). Y_2TiO_5 was identified with PDF card no. 00-027-0981; $CaAl_2Si_2O_8$ with PDF card no. 00-041-1486.

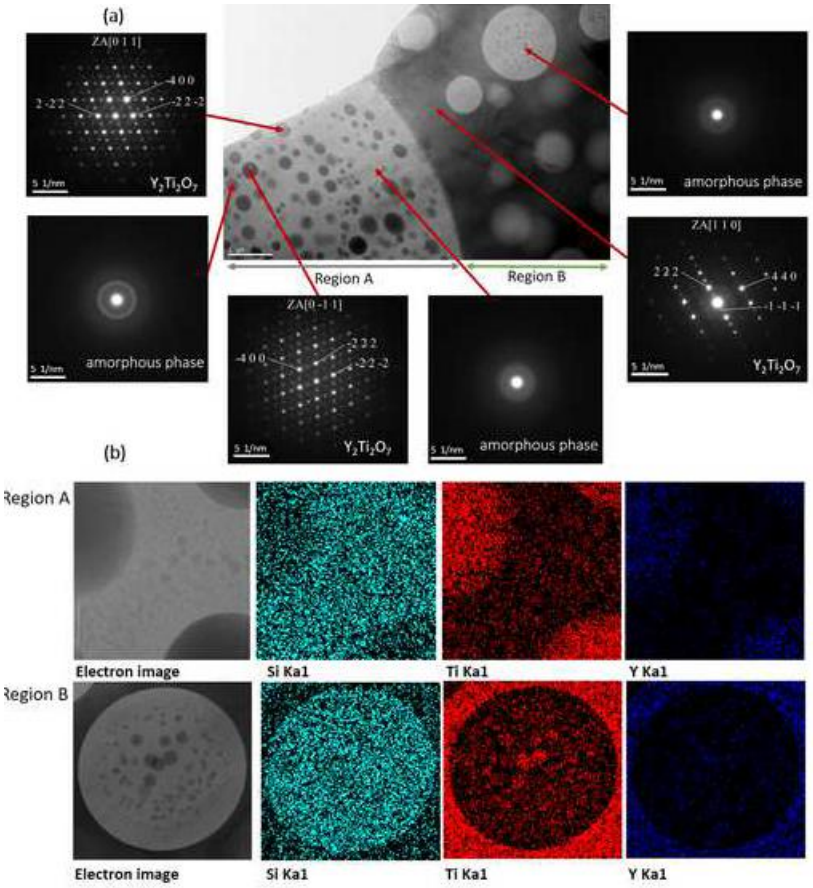

Figure 3: (a) TEM and SAED analyses of the as-cast T1; (b) EDS mapping of a selected area in region A and region B.

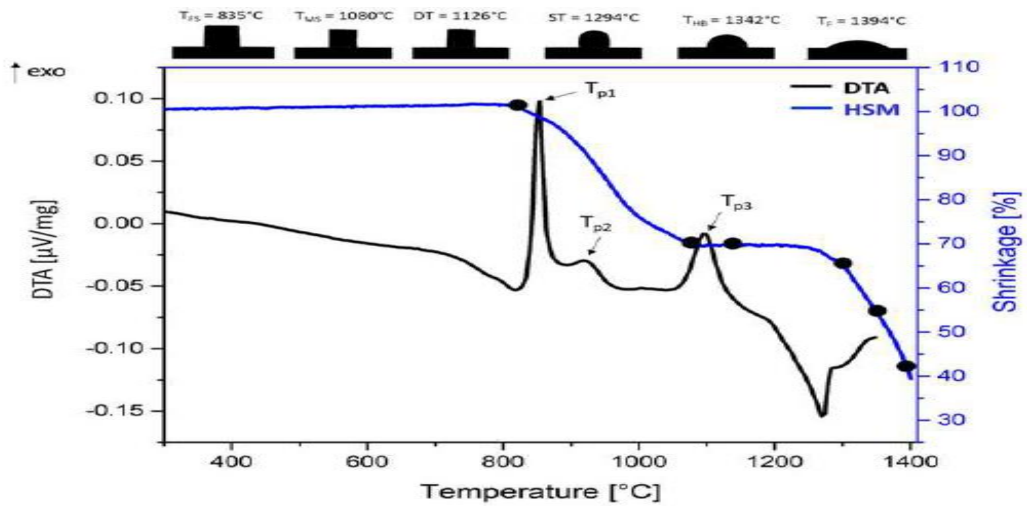

Figure 4: DTA (black) and HSM (blue) curves of the T1 glass (10 °C/min heating rate) and T1 powder size < 38 µm.

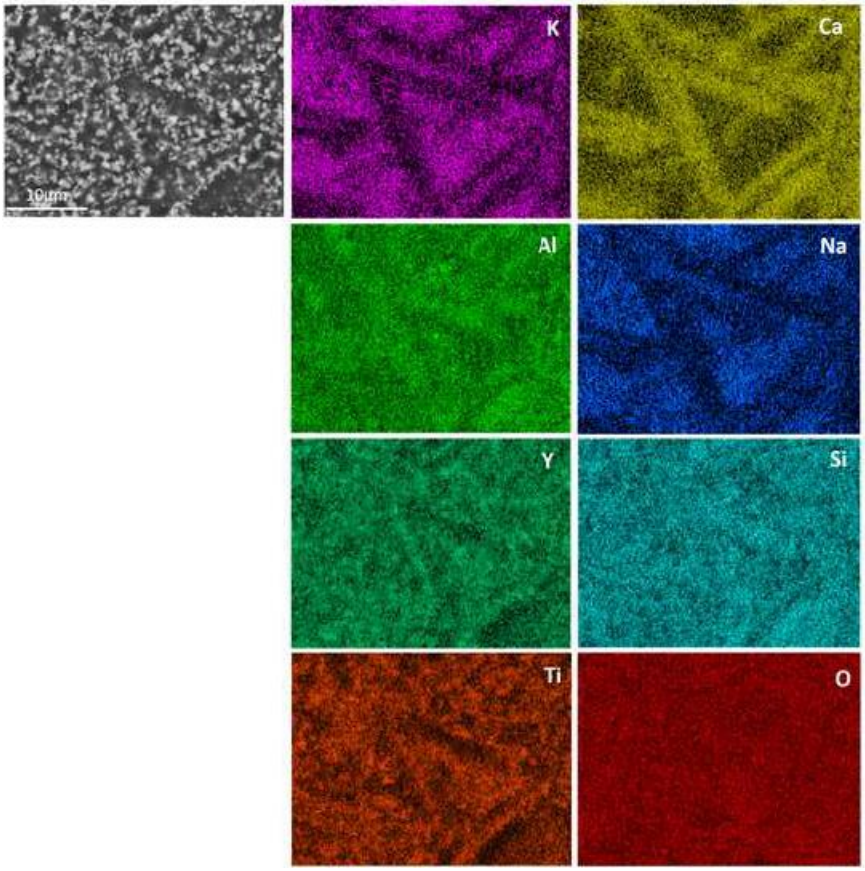

Figure 5: (a) SEM (BSE) analysis of a T1 glass-ceramic pellet (sintered at 1300 °C for 10 min and 855 °C for 30 min, Ar flow) and (b) the related EDS elemental maps.

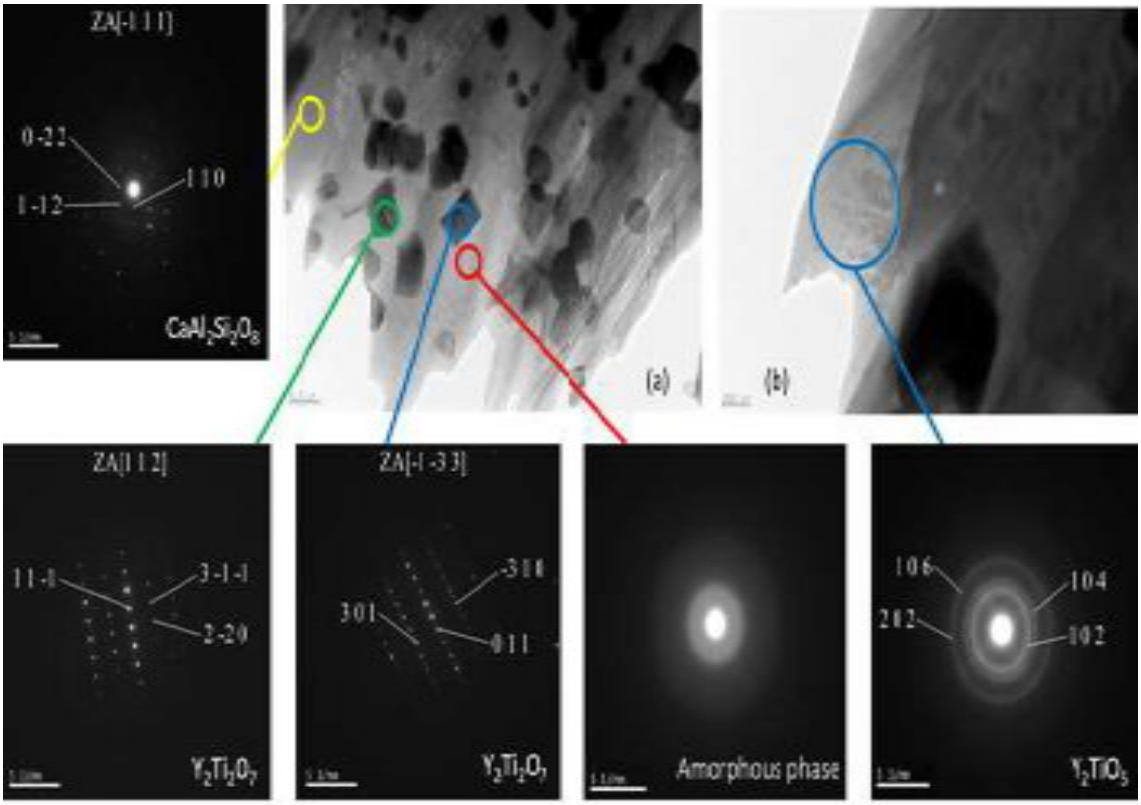

Figure 6: TEM and SAED analyses of the T1 glass-ceramic pellet (sintered at 1300 °C for 10 min and 855 °C for 30 min, Ar flow).

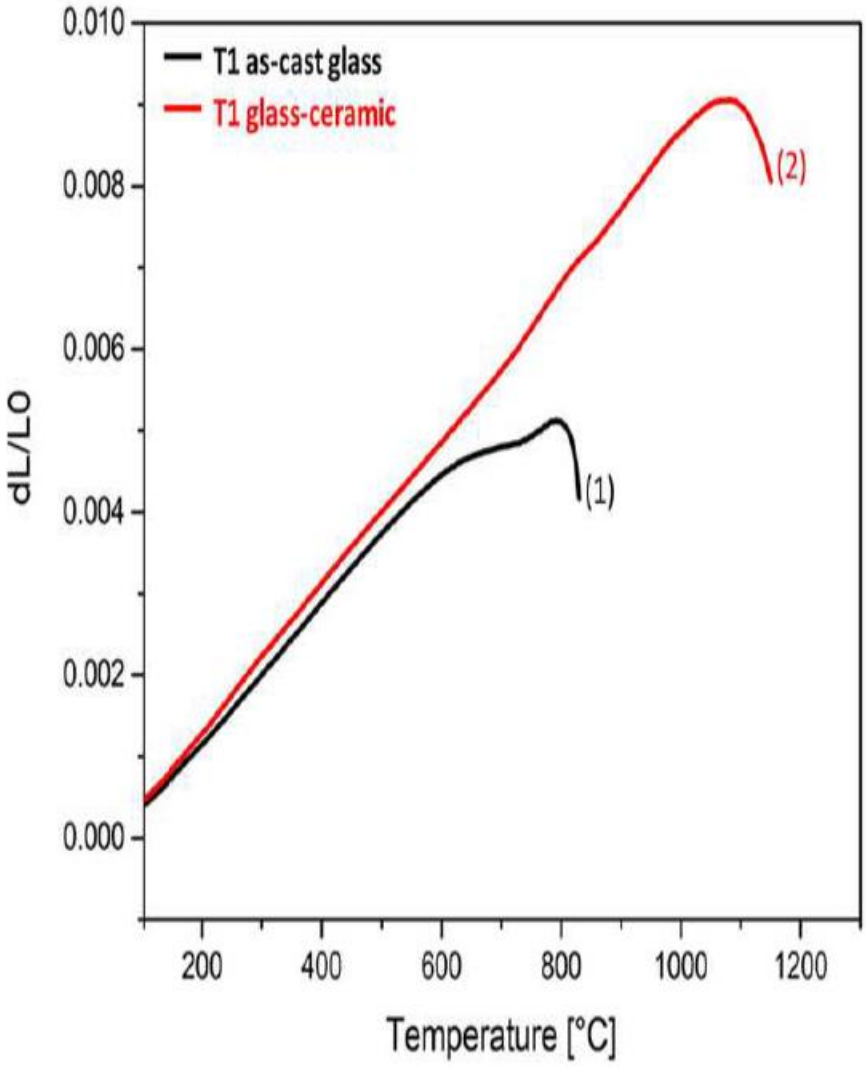

Figure 7: Dilatometry curves of the T1 glass (curve 1) and T1 glass-ceramic obtained after curing at 1300 °C for 10 min, followed by a heat-treatment at 855 °C for 30 minutes (curve 2); 5 °C/min heating rate.

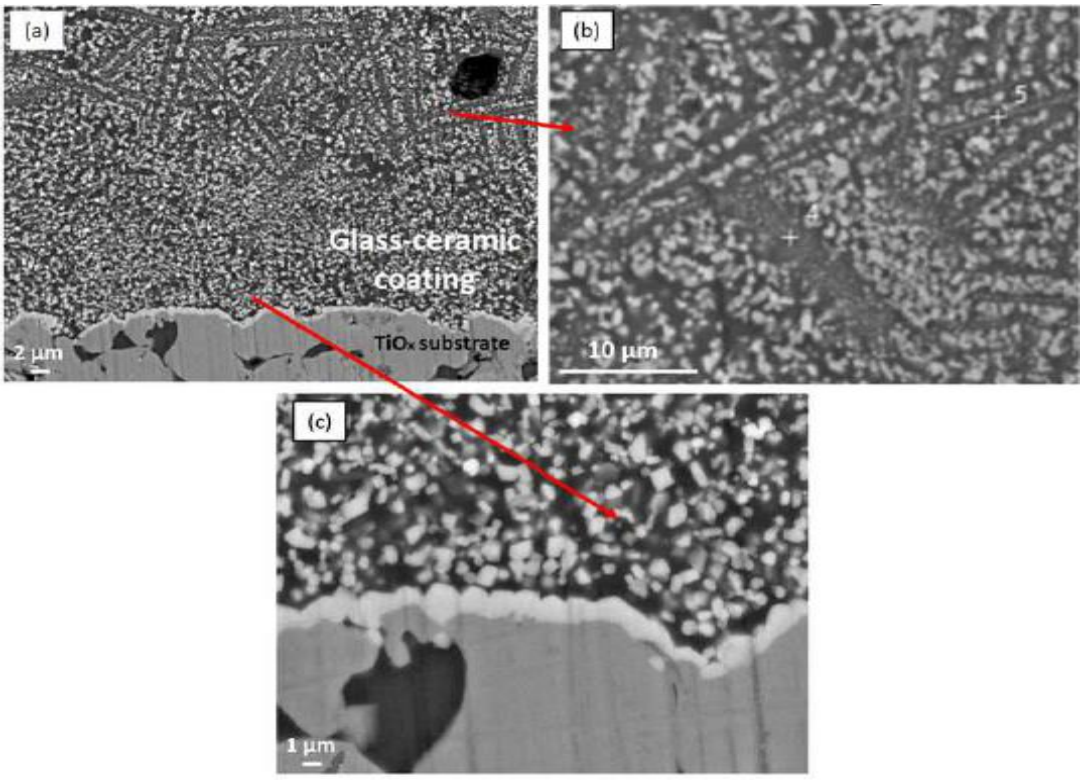

Figure 8: SEM images (BSE) of (a) the cross-section of a T1 glass-ceramic coated TiOx, (b) the T1 coating at a distance of ~ 20 µm from the T1/TiO_x interface, and (c) close to the T1/TiOx interface.

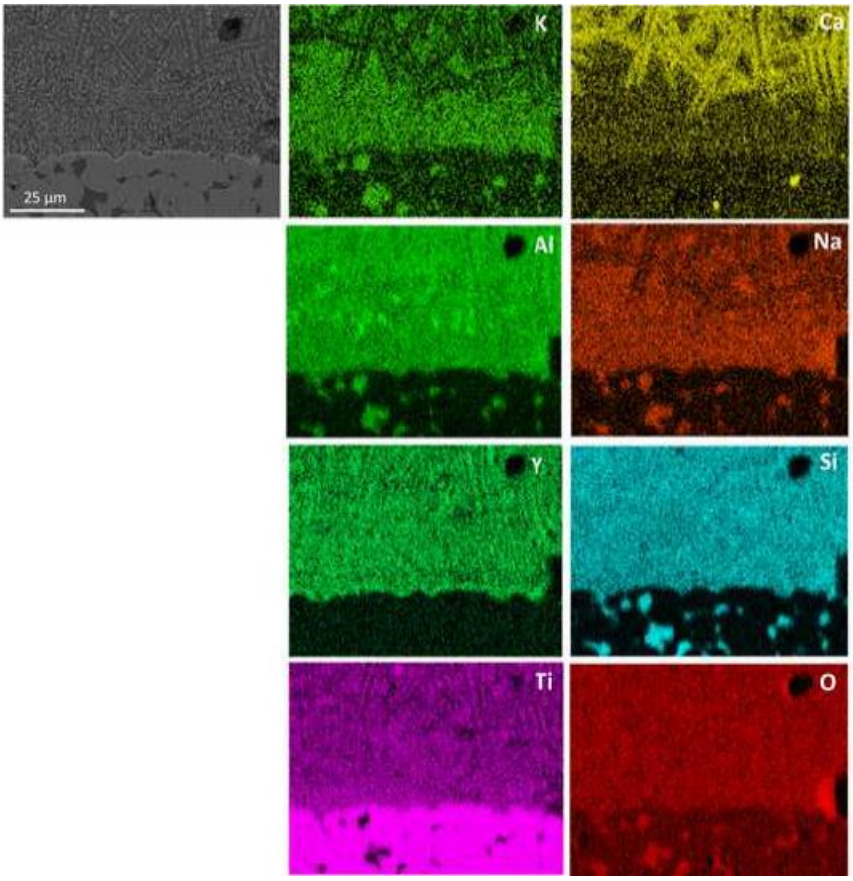

Figure 9: SEM image of the T1 glass-ceramic/TiO_x interface substrate with the related EDS elemental maps.

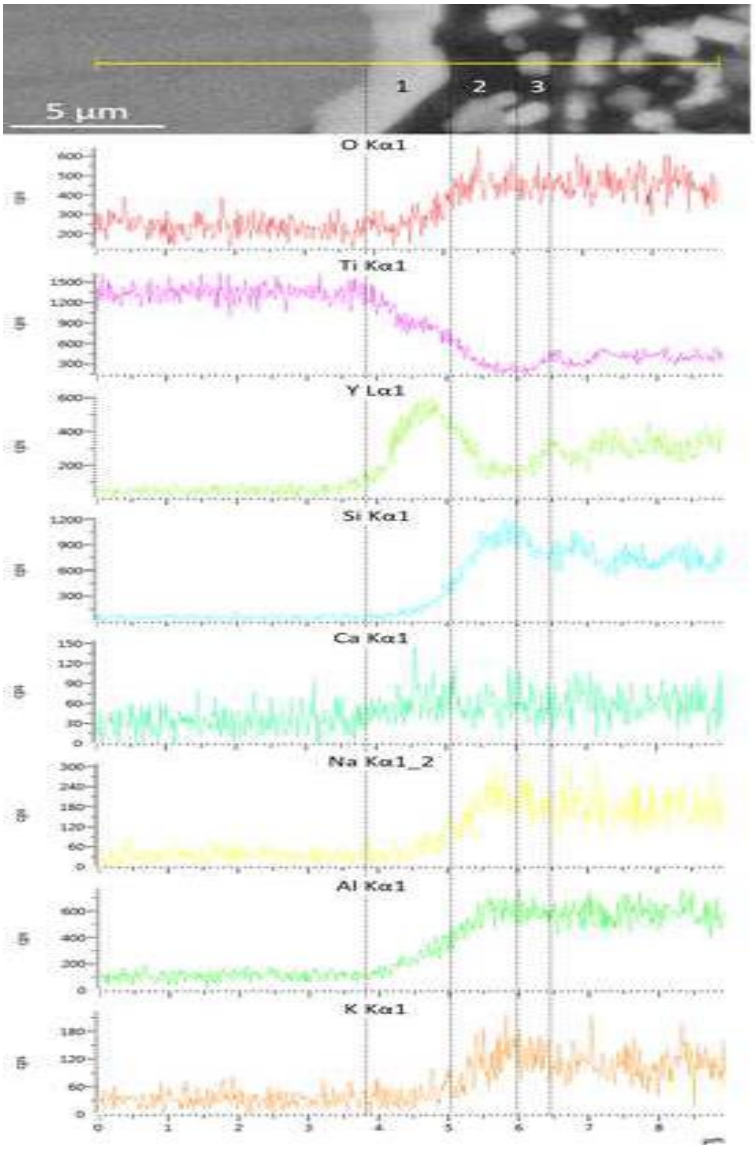

Figure 10: EDS line-scan at the TiO_x/T1 glass-ceramic interface.

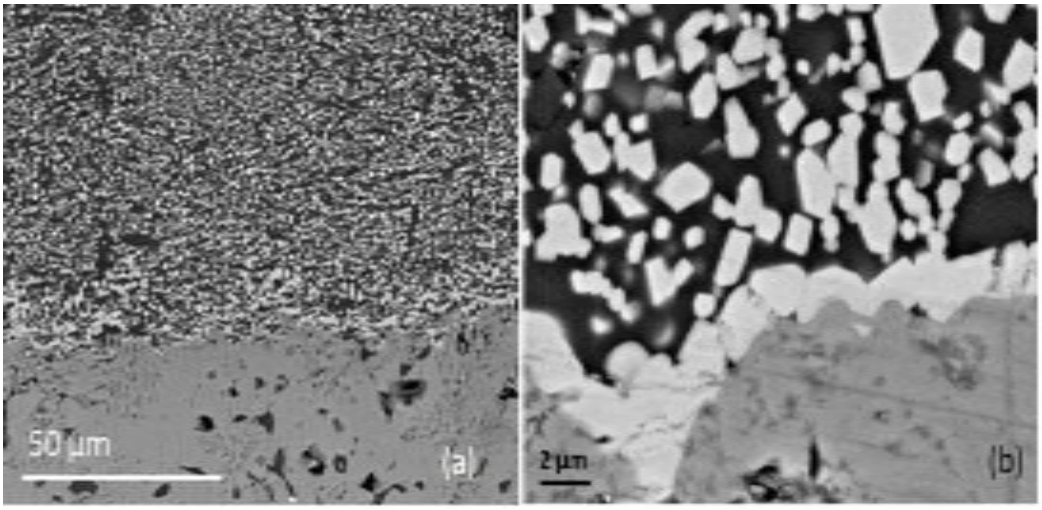

Figure 11: SEM images (BSE) of (a) the cross-section of a T1 glass-ceramic coated TiO_x and (b) close to the T1/TiO_x interface, after the oxidation test at 600 °C for 120 h.

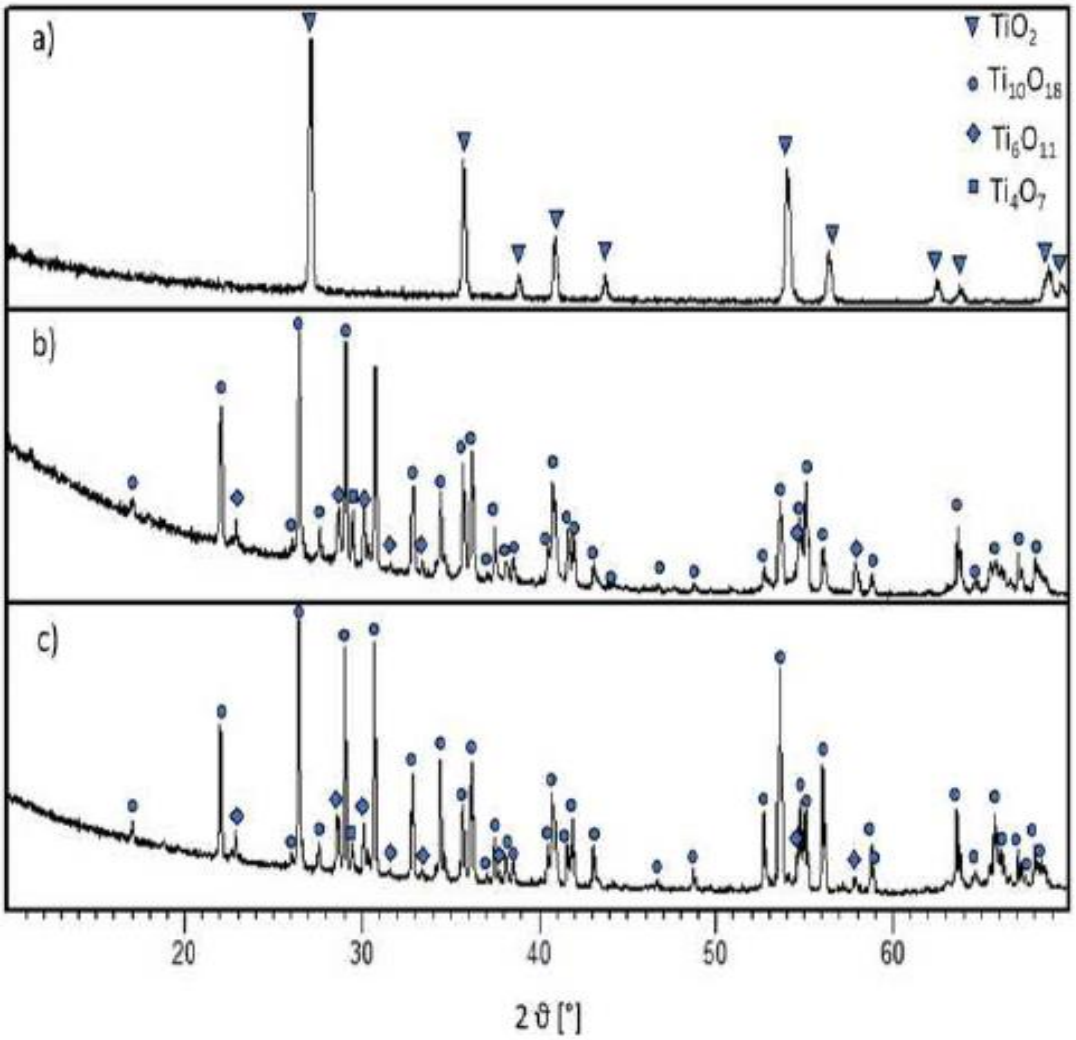

Figure 12: XRD patterns of (a) uncoated TiO_x after the oxidation test at 600 °C for 120 h in air, (b) T1 glass-ceramic coated TiO_x after the oxidation test at 600 °C for 120 h in air, and (c) as-sintered TiO_x.

Table 1: Characteristic temperatures of the T1 glass (< 38 µm powder size) measured by means of DTA (10 °C/min heating rate). T_g: glass transition temperature; T_x: temperature corresponding to the onset of the crystallisation peak; T_p: temperature corresponding to the crystallisation peak; T_m: melting temperature.

	T_g	T_{x1}	T_{p1}	T_{x2}	T_{p2}	T_{x3}	T_{p3}	T_m
T1 glass	752°C	819°C	852°C	884°C	919°C	1046°C	1097°C	1271°C